Journal of the European Ceramic Society 22 (2002) 2901–2909

www.elsevier.com/locate/jeurceramsoc

Preparation of zircon bodies from amorphous precursor powder synthesized by sol-gel processing

C. Veytizou, J.F. Quinson*, Y. Jorand

Laboratoire GEMPPM, UMR CNRS 5510, Batiment Blaise Pascal, INSA, 20 Avenue Albert Einstein, 69621 Villeurbanne Cedex, France

Received 12 July 2001; received in revised form 2 February 2002; accepted 24 February 2002

Abstract

Comments concerning both synthesis conditions and characteristics of the amorphous zircon precursor powder, which already have been published, lead us to propose a schematic representation of powder grains. The sintering of the precursor powder during the calcination treatment is similar to a "moderate" sintering, which can be justified by the different nature of primary particles composing the grains. The sintering of green bodies prepared from the precursor powder compacted then isostically pressed, is possible at temperatures as low as 1200 °C. The sintered bodies exhibit a high relative density, close to 95%, but their microstructure reveals the presence of cracks that the morphology of synthesized zircon could be sufficient to justify.

Keywords: Sol-gel processes; Sintering; Microstructures-final; $ZrSiO_4$; Precursors-organic

1. Introduction

It is well known that zircon is a very interesting refractory material for high temperature applications. Indeed, this silicate exhibits attractive properties, such as low thermal expansion, low thermal conductivity, and high resistance to thermal shock. However to take the best advantage of these properties, zircon should be highly pure: the presence of impureties as Al_2O_3, Fe_2O_3, TiO_2, and SiO_2 has disastrous consequences on the thermomechanical behaviour of sintered bodies prepared from natural zircon sands.[1]

Although difficult, the preparation of high-purity $ZrSiO_4$ has already been the subject of a great number of research papers.[2–11] Unfortunately, the full densification of synthetised zircon was never observed, even at temperatures higher than 1600 °C.[7,12]

The purpose of this work was to study the sintering behaviour of an amorphous zircon precursor powder synthesized by sol-gel processing.[13]

1.1. State of the art

The zircon synthesis as well as the characterization of the two intermediate steps of obtaining, i.e. the sol and the zircon precursor powder have already been presented.[13] Consequently, only a brief review is reported here.

1.1.1. Synthesis

Zircon powders were prepared from tetraethoxysilane (TEOS), $Si(OC_2H_5)_4$, and zirconyl nitrate hydrate, $ZrO(NO_3)_2\ 6H_2O$, mixed in water in a stoechiometric ratio. The starting solution corresponds to a concentration of 0.12 mol l^{-1} of zircon, with a high $[H_2O]/[TEOS]$ molar ratio equal to 450. Considering the high dilution and the very low pH (~1) exhibited by the aqueous solution of zirconyl nitrate, TEOS is rapidly hydrolysed into silica acid, $Si(OH)_4$: so, a reactive precursor solution of zirconyl nitrate and silica acid is formed. Refluxed at 100 °C for 24 h, this solution is turned into a colloïdal sol. The latter is precipitated in a diluted ammonia solution to form a gel, which is filtered, washed to eliminate reactional residues, then dried at 100 °C to be converted into a zircon precursor powder.

1.1.2. Zircon precursor powder characterization

It is shown by Raman spectroscopy that Zr–O–Si bonds are formed in situ when the starting solution is heated to reflux at 100 °C.

* Corresponding author.
E-mail address: jean-francois.quinson@wanadoo.fr (J.F. Quinson).

0955-2219/02/$ - see front matter
PII: S0955-2219(02)00038-9

X-ray and ^{29}Si MAS NMR characterization of the precursor powder confirms the presence of the zircon network at low temperature (Fig. 1). In addition to the sharp signal at −82.00 ppm due to the single Si site in zircon, the NMR spectrum exhibits a broad peak centered at −92 ppm. The latter is characteristic of a siliceous phase, principally composed of Q_2 units. Moreover, a quantitative ^{29}Si MAS NMR analysis reveals that the zircon yield detected in the precursor powder reaches 15% for a reflux time of 24 h.

N_2 adsorption–desorption measurements at 77 K used to characterize the porous texture of the precursor powder lead to a type IV isotherm with a H_2-type hysteresis loop (Fig. 2), which indicates the presence of "ink-bottle" mesopores or, more probably, of spheroidal mesoporous cavities with narrow necks, created by a packing of spherical-like particles.[14]

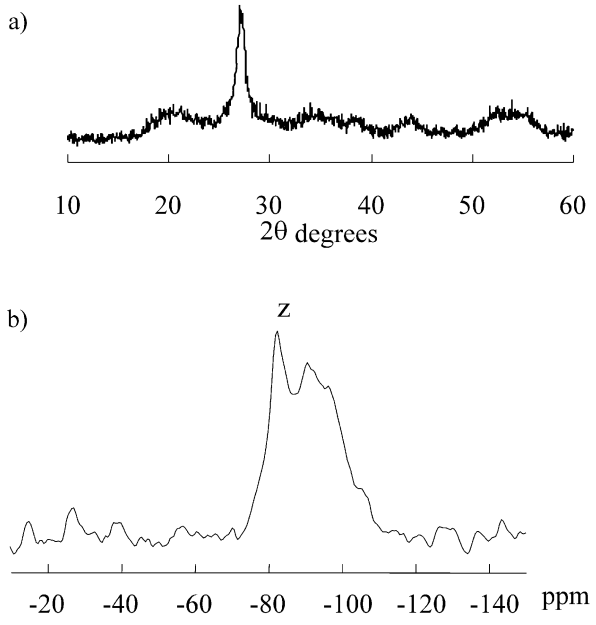

Fig. 1. XRD (a) and ^{29}Si MAS NMR (b) spectra of the precursor powder. z = zircon.

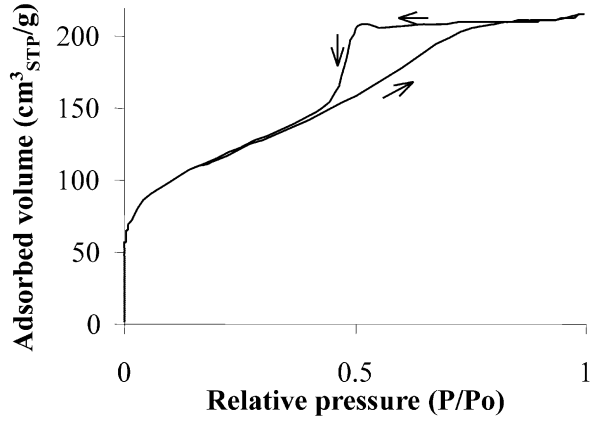

Fig. 2. N_2 adsorption–desorption isotherm measured on the precursor powder.

The textural data of the precursor powder are given in Table 1.

Table 1
Textural data of the precursor powder

$S_{B\cdot E.T.}$ (m^2/g)	V_{micro} (mm^3/g)	V_{meso} (mm^3/g)	$R_{V/2}$ (nm)	ΔR (nm)
412	27	274	2.15	0.8–5

$S_{B\cdot E.T.}$:surface area; V_{micro}:microporous volume; V_{meso}: mesoporous volume; $R_{V/2}$: mean pore radius corresponding to 50% of the mesoporous volume; ΔR: pore size interval.

It should be noted that:

- Mesopore radius and mesoporous volume are deduced from the adsorption branch of the isotherm, applying the B.J.H. method based on the Kelvin equation.[15] Indeed, the desorption branch of the isotherm, usually used for such a measurement, allows only the determination of the neck size and so provides an erroneous picture of the mesoporous texture.
- Surface area and microporous volume are also determined using the B.E.T. method[16] and the t-method,[17] respectively.

SEM examination of the precursor powder prior to calcination (Fig. 3a) shows both irregularly shaped and differently sized agglomerates or aggregates. Granulometric analysis reveals a broadened volume particle-size

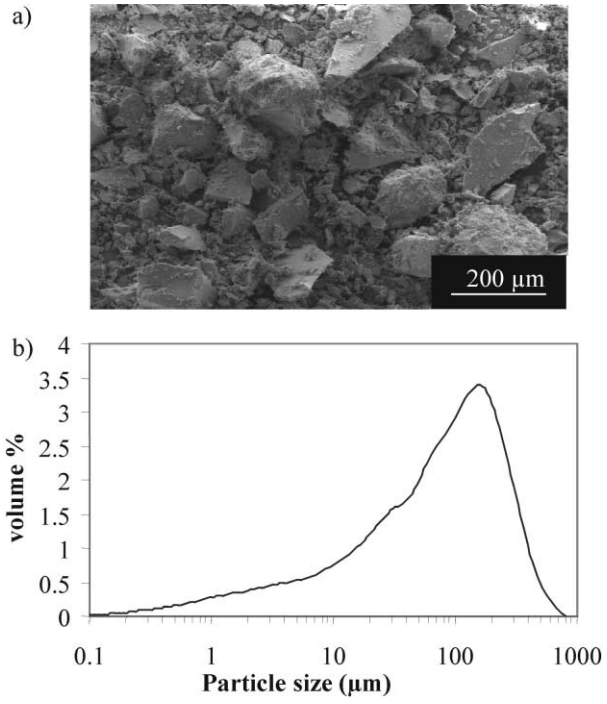

Fig. 3. Precursor powder morphology: (a) SEM micrograph and (b) volume particle-size distribution.

distribution, varying from 0.1 to 800 μm (Fig. 3b). The large particles observed are related to aggregates probably resulting from rinsing with water carried out in order to eliminate ammonium nitrate formed during sol precipitation.

2. Results

2.1. Sintering of the precursor powder

2.1.1. Structural representation of the powder grain

The different results summarized above (Section 1.1) give rise to some comments, which lead us to propose a schematic representation of the powder grain.

Considering the low percentage of zircon formed inside the sol after 24 h under reflux, the presence of siliceous and zirconyl species is obvious. In view of information given by the literature, both concerning the polymerization of silicic acid in an aqueous medium[18] and the structure of the zirconyl nitrate hydrate,[19] we may conclude that:

- the siliceous species correspond to cyclic oligomers formed of structural units in which each Si atom is surrounded with two siloxane bonds and two silanol bonds (i.e. Q^2 units).
- the zirconyl species identify with the macrocations $[Zr(OH)_2(H_2O)_2NO_3]^+$, which constitute the structure of zirconium hydroxide nitrate. These macrocations are assumed unmodified during the treatment under reflux, both because of an equivalent amount of nitrate counterions and a very low pH ($\sim$1).

It is worth noting that the in-situ formation of Zr–O–Si bonds is made possible by a condensation reaction between silicic acid and some macrocations, via the hydroxyl groups linked to zirconium and silicon atoms.

When the refluxed sol is precipitated in a dilute ammonia solution, the siliceous and zirconyl species undergo modifications owing to increasingly strong pH: an aggregation of hydroxylated silica oligomers, as well as a precipitation of macrocations to amorphous hydrous zirconia due to the release of nitrate ions chelated to zirconium atoms,[20] must occur. Over the same time, owing to the formation of Zr–O–Si bonds during the reflux treatment and, possibly, during the precipitation step, zircon associated to amorphous zirconia is obtained.

After drying at 100 °C, the colloidal precipitate is transformed into the precursor powder whose grains consist of primary particles of hydroxylated silica, of amorphous zirconia whether or not combined with zircon. Information deduced from textural analysis, previously mentioned, specify that these particles may be considered like spheres. Moreover, the kinetic study of zircon formation, published elsewhere,[21] reveals that the low yield of detected zircon is present as a crown at the surface of some zirconia particles.

2.1.2. Sintering

The textural evolution of the precursor powder during the calcination treatment was investigated using the N_2 adsorption-desorption technique. Experiments were performed at 77 K on samples previously calcined under air for 1 h, in the 600–1300 °C temperature range, then outgassed at 200 °C for 3 h.

The different textural characteristics obtained are reported in Fig. 4, and Table 2.

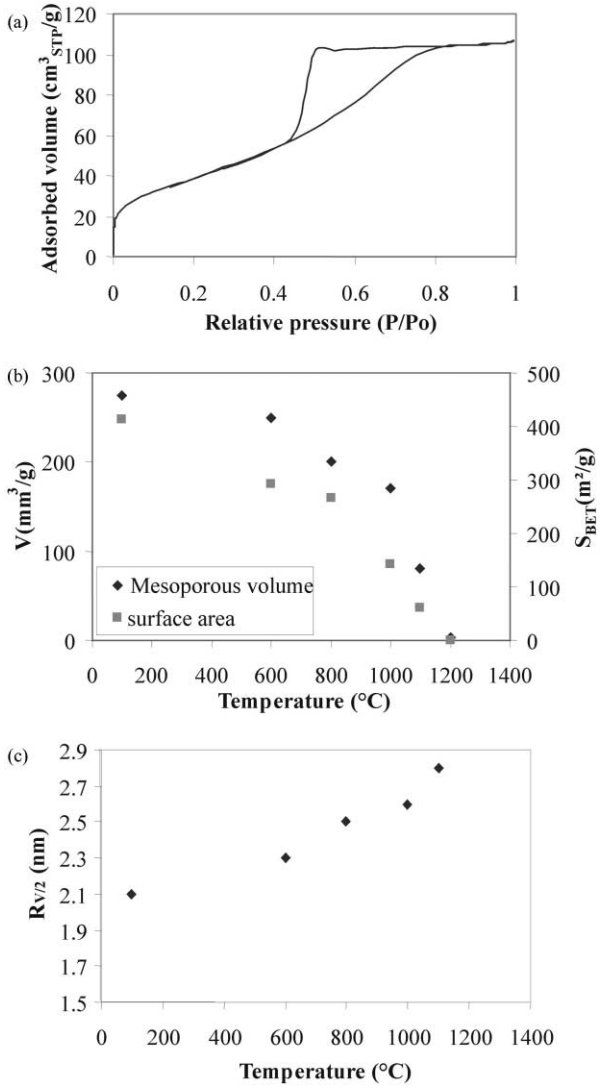

Fig. 4. (a) N_2 adsorption-desorption isotherm measured on the precursor powder calcined at 1000 °C, given as an example. (b) Mesoporous volume and surface area evolution as a function of the calcination temperature. (c) Mean pore radius evolution as a function of the calcination temperature.

Table 2
Evolution of the pore size interval, ΔR, as a function of the calcination temperature

Temperature (°C)	R_{max} (nm)	R_{min} (nm)	ΔR (nm)
100	5.85	0.85	5
600	5.7	0.85	4.85
800	6.35	0.85	5.5
1000	5.85	0.9	4.95
1100	5.65	1.05	4.6

Whatever the calcination temperature, it is important to underline that the adsorption–desorption isotherm as well as the hysteresis loop (Fig. 4a) exhibit a shape identical to that found when the precursor powder is dried only (Fig. 2) In particular, this observation suggests that the pore morphology and, consequently, that of primary particles whose packing inside the powder grain generates mesopores, are not affected during the sintering.

On the other hand, a large modification of the mesoporous texture is detected after each calcination treatment (Figs. 4b, c and Table 2):

- from 600 °C, total disappearance of the microporosity
- up to 1200 °C, fast decrease of surface area and of mesoporous volume combined with a slow increase of mean pore radius, which practically does not affect the spreading, ΔR, of the pore radius distribution curve.

This textural evolution seems to indicate that the sintering of the precursor powder is similar to a "moderate" sintering,[22] which is distinguished by a localized size increase of primary particles composing the grains, without bringing about an appreciable variation of the mean pore radius. Such a process can be justified by the different nature of primary particles.

- from 1200 °C, total disappearance of the mesoporosity leading to the formation of dense powder grains. It should be noted that the precursor powder is entirely converted to zircon at this temperature.

2.2. Sintering of the green body

2.2.1. Shaping conditions

The first step to prepare ceramics from powders is shaping which leads to a green body. Generally, the process used is compaction: the powder is placed in a mould, then a uniaxial pressure is applied. This method allows us to obtain cylindrical green bodies whose density can be determined geometrically. The response curve, relative green density versus compaction pressure[23] is presented in Fig. 5. It should be noted that the relative green density does not exceed 48% of precursor powder density measured by helium pycnometry ($d=3$). This value is too low to hope that a good sintering density can be attained. It can be increased by isostatically pressing the compacted samples. In this way, a relative density close to 70% is reached for a 300 MPa isostatic pressure (Fig. 6).

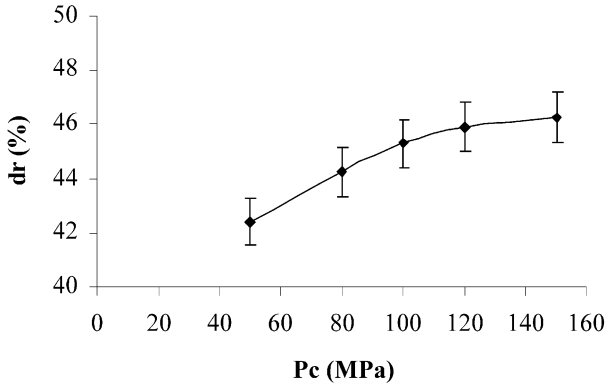

Fig. 5. Relative density of green bodies versus compacting pressure.

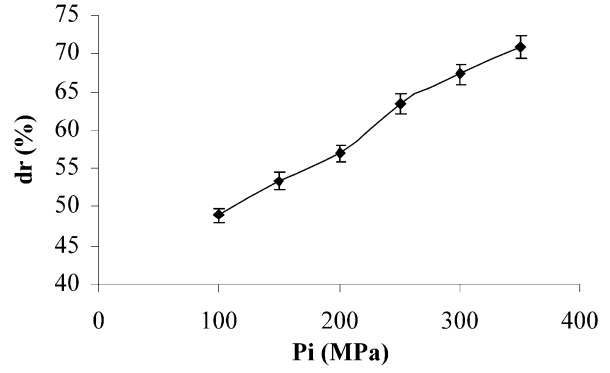

Fig. 6. Relative density of compacted green bodies versus isostatic pressure.

2.2.2. Sintering conditions

The sintering study was realized in an air atmosphere up to 1500 °C, by means of a TM92 Setaram dilatometer. The shrinkage was measured on the perpendicular axis with regard to the plane faces of green bodies, during a heat treatment at 5 °C/mn. Dilatometric curve (Fig. 7) reveals that the shrinkage proceeds within three steps:

- The first one, up to 1000 °C, is associated to weight loss (water and ammonium nitrate elimination) and to powder sintering.

- The second, between 1000 and 1200 °C, is faster because intergranular sintering, combined with the powder crystallization, is superimposed on intragranular sintering.
- The last, beyond 1200 °C, is only due to intergranular sintering, given that the densification of powder grains is achieved.

At the same time, it is worth noting that the volume shrinkage is very large (~65%) during sintering and that the relative density of sintered bodies is high since it is equivalent to 95% of synthesized zircon powder density, measured by helium pycnometry ($d=4.$).

Remark: the relative density of green bodies, which are only compacted, does not exceed 77% after sintering. This result demonstrates that the isostatic pressing step is essential to obtain dense samples.

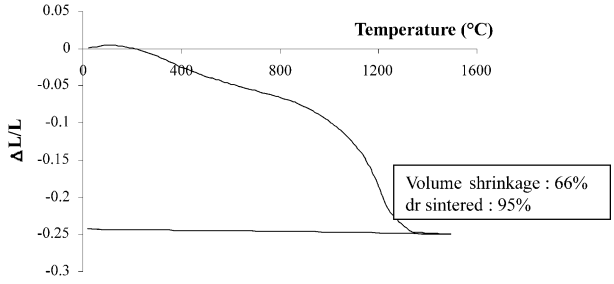

Fig. 7. Dilatometric curve of a green body of 70% relative density, obtained by heating up to 1500 °C.

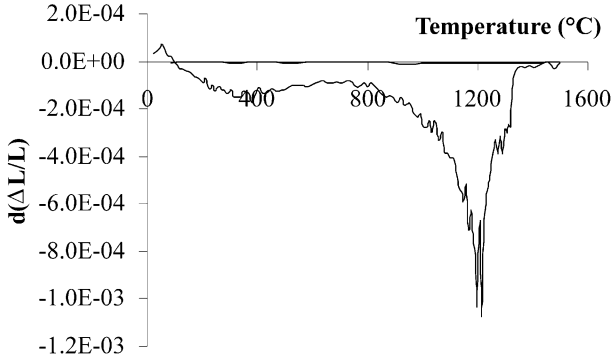

Fig. 8. Derivative dilatometric curve of a green body of 70% relative density.

According to the derivative dilatometric curve shown in Fig. 8, the sintering rate is maximum for 1200 °C. Therefore, this temperature is chosen to sinter the green bodies. At 1200 °C, a holding time for 6 h is necessary to obtain both the densification and the total transformation to zircon (Fig. 9).

A sintering temperature as low as 1200 °C is justified by the high reactivity and the amorphous state of the precursor powder.

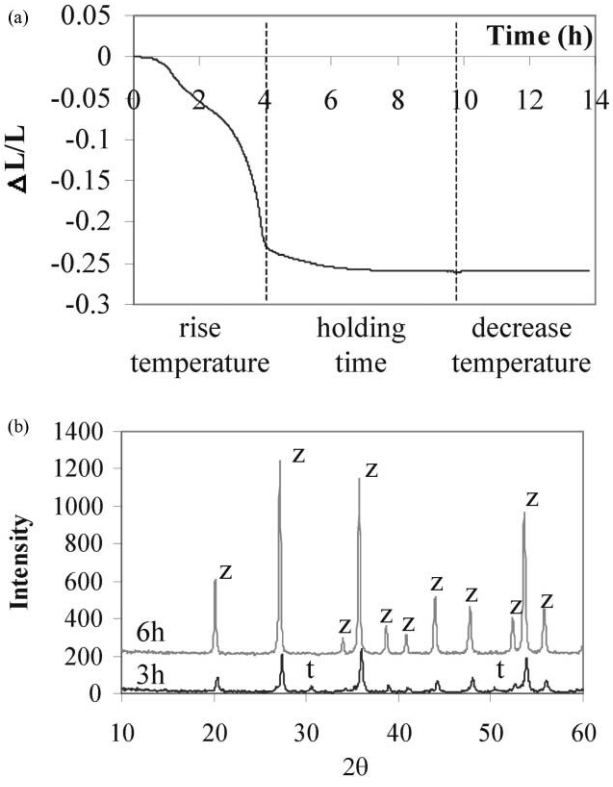

Fig. 9. (a) Dilatometric curve obtained by heating up to 1200 °C then holding (b) XRD diagrams after 3 and 6 h. t = tetragonal zirconia; z = zircon.

2.2.3. Sintered body characterization

It should be noted that green bodies are first heated slowly up to 400 °C to eliminate synthesis residues, before sintering under air for 6 h at 1200 °C.

The pore size distribution of the sintered bodies is measured by mercury porosimetry . Two pores population are detected (Fig. 10):

- mesopores inside the diameter range 10^{-1} and 10^{-2} μm, which correspond to 5% of residual intergranular porosity.

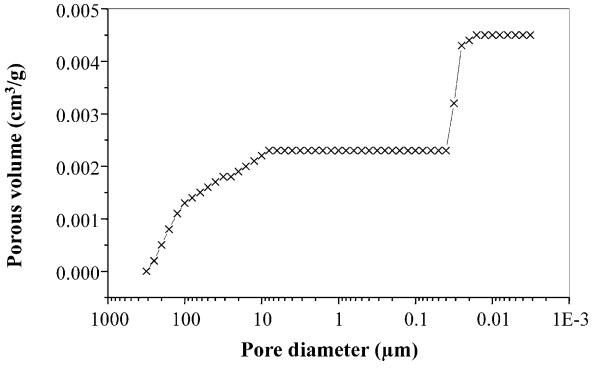

Fig. 10. Pore size distribution of sintered bodies measured by mercury porosimetry.

- macropores, having a diameter larger than 10 μm, attributed to cracks present on the surface.

After polishing with diamond suspension down to 1 μm then heating at 1180 °C for 6 h to reveal the grains, six sintered samples of which some characteristics are given in Table 3, were observed by scanning electron microscopy (SEM). The SEM micrographs (Fig. 11) reveal the formation of cracks for isostatic pressures greater than 200 MPa. According to Table 3, this last observation means that the sintered bodies are crack-free insofar as their relative density does not exceed 90%.

Table 3
Characteristics, before and after sintering, of samples prepared from the precursor powder[a]

Samples	A		B		C		D		E		F	
	G	S	G	S	G	S	G	S	G	S	G	S
Pc(MPa)	100		100		100		100		100		100	
Pi(MPa)	100		150		200		250		300		350	
dr(%)	49	81	54	85	57	90	63	92	67	94	71	95
$\Delta V/V$(%)	68		67		67		64		62		60	

[a] G: Green, S: Sintered. Pc: compaction pressure, Pi: isostatic pressure, dr: relative density, $\Delta V/V$: volume shrinkage.

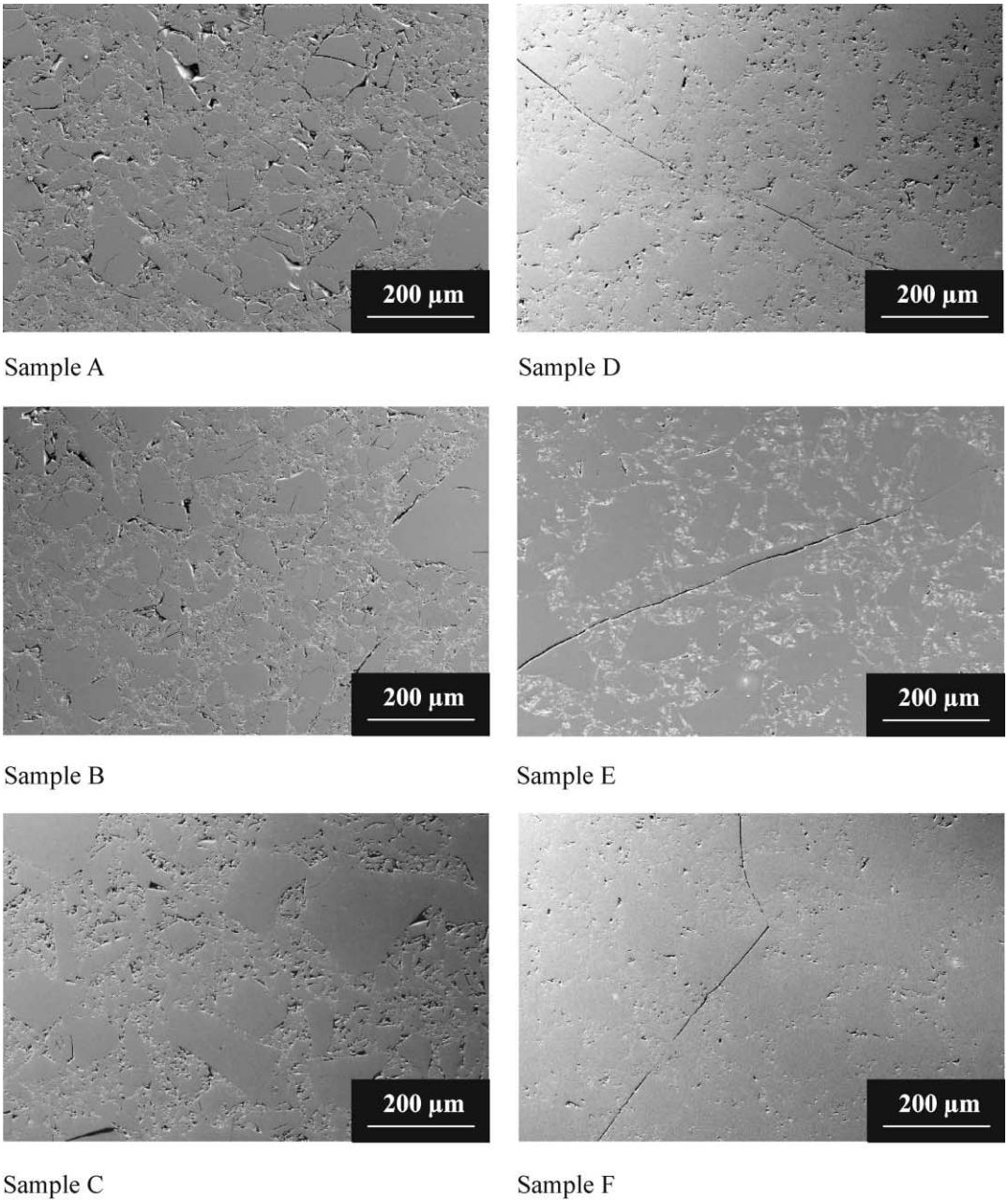

Fig. 11. SEM micrographs of sintered bodies prepared from the precursor powder, formed using different isostatic pressures.

3. Discussion

The cracking of sintered samples is due to internal stresses generated during shaping and /or sintering. Different causes were investigated to explain their origin:

- Morphology of the precursor powder.

Given the irregular shape and the different size of grains, their reorganisation during powder shaping is assumed to create stresses inside green bodies. To remedy this problem, an amorphous zircon powder with controlled morphology was prepared by spray-drying.[13] In this case, spherical particles in the diameter range 0.2–10 μm were produced (Fig. 12).

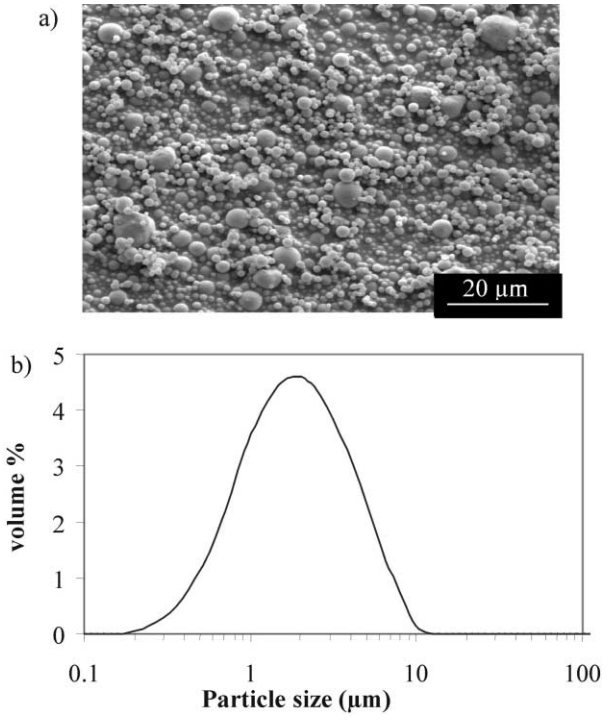

Fig. 12. Powder produced by spray-drying: (a) SEM micrograph and (b) volume particle-size distribution.

As for the precursor powder, the shaping of the spray-dried powder involves successively, compaction and isostatic pressing steps. The sintering of so prepared green bodies leads to pellets whose the relative density does not exceed 85% (Table 4) and generates cracks whatever the applied isostatic pressure as shown by SEM analysis (Fig. 13).

Contrary to all expectation, the control of shape and the size of powder grains is not sufficient to obtain crack-free sintered bodies.

Table 4
Characteristics, before and after sintering, of samples prepared from powder produced by spray-drying[a]

Samples	A		B		C		D		E		F	
	G	S	G	S	G	S	G	S	G	S	G	S
Pc(MPa)	120		120		120		120		120		120	
Pi(MPa)	100		150		200		250		300		350	
dr(%)	52	72	58	79	61	81	67	83	71	85	71	85
$\Delta V/V$(%)	62		61		60		60		57		56	

[a] G: Green, S: Sintered. Pc: compaction pressure, Pi: isostatic pressure, dr: relative density, $\Delta V/V$: volume shrinkage.

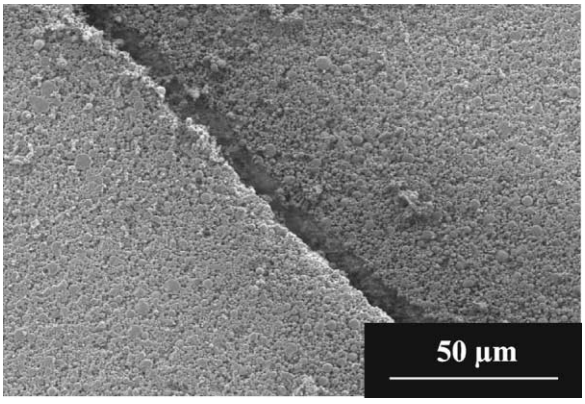

Fig. 13. SEM micrograph of a sintered body (sample A, Table 4), prepared from spray-dried powder and formed applying a low isostatic pressure (100 MPa).

- Volume shrinkage

During sintering, a large volume shrinkage is noted (~60%), which contributes to create strong stresses inside the samples. To reduce these stresses, a dilatometric analysis based on the shrinkage control was performed: the chosen shrinkage rate is very low and equal to 0.06%/mn, which corresponds only to 1/10 of the maximum shrinkage rate recorded when the sample is heated at a rate of 5 °C/mn. Under these conditions, a stress limitation destined to avoid the crack formation was expected. Unfortunately, such an approach still leads to a cracked sample after sintering (Fig. 14).

- Crystallization of the precursor powder.

The structural evolution of the amorphous precursor powder with heat treatment reveals that the zircon formation is possible from 1150 °C by reaction between amorphous silica and tetragonal zirconia formed from 1000 °C.[21] The successive crystallizations of zirconia and of zircon, that take place during sintering, might

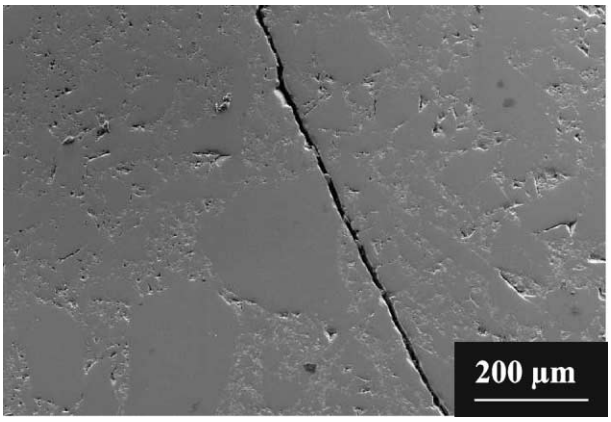

Fig. 14. SEM micrograph of a green body sintered by controlling shrinkage.

bring about stresses at the origin of cracking of sintered samples. Indeed, this assumption cannot be taken into consideration, given that the SEM observation of a crystallized zircon body prepared from precursor powder calcined at 1300 °C and sintered by hot pressing at 1600 °C in a nitrogen atmosphere, always indicates the presence of cracks (Fig. 15).

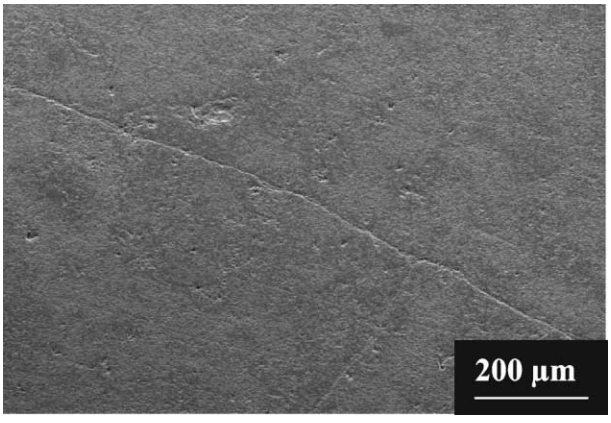

Fig. 15. SEM micrograph of a crystallized zircon body sintered by hot pressing at 1600 °C.

- Intrinsic properties of zircon powder.

A TEM observation shows that powder grains of sintered zircon bodies are formed of very small crystallites, oriented differently (Fig. 16). Such a microstructure can explain by itself the existence of stresses and so justify the persistent presence of cracks.

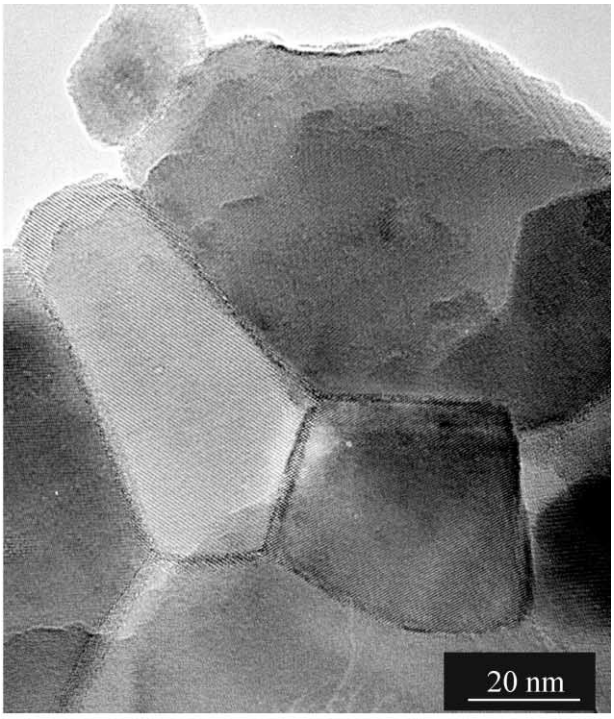

(a)

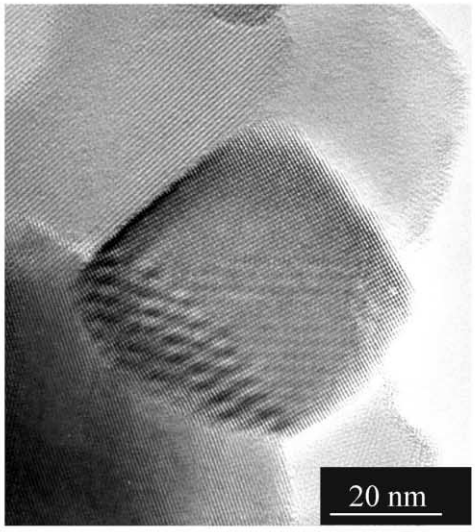

(b)

Fig. 16. (a) and (b) TEM micrographs of the precursor powder.

4. Conclusion

From an amorphous precursor powder synthesized by a sol-gel process, it is possible to elaborate at low temperatures, pure zircon exhibiting a high relative density (95%). Unfortunately, the sintered bodies are always cracked. Among the different causes invoked to explain the formation of such cracks, the presence of stresses inherent in the morphology of synthesized zircon seems to be the most probable.

References

1. Carbonneau X. *Etude des propriétés thermomécaniques de mullite zircone et de zircon*, Thèse sci: INSA de Lyon, 1997.
2. Mosset, A., Baules, P., Lecante, P., Trombe, J. C., Ahamdane, H. and Bensamka, F., A new route to silicates, Part 4—submersion zircon powders. *J. Mater. Chem.*, 1996, **6**(9), 1527–1532.
3. Valero, R., Durand, B., Guth, J. L. and Chopin, T., Mechanism of hydrothermal synthesis fluoride medium: hydrothermal synthesis of zircon. *J. Sol-Gel Sci. Technol*, 1998, **13**, 119–122.
4. Kanno, Y. and Suzuki, T., Estimation of formation mechanism of spherical fine ZrO_2–SiO_2 particles by ultrasonic spray pyrolysis. *J. Mat. Sci. Lett.*, 1988, **7**, 3067–3072.
5. Kanno, Y., Thermodynamic and cristallographic discussion of the formation and dissociation of zircon. *J. Mater. Sci.*, 1989, **24**, 2415–2420.
6. Kobayashi, H., Terasaki, T., Mori, T., Yamamura, H. and Mitamura, T., Preparation of $ZrSiO_4$ powders by sol-gel process (Part 3)—preparation conditions of $ZrSiO_4$ composition precursor gels from $Si(OC_2H_5)_4$ and $Zr(O^iC_3H_7)_4$ alkoxydes. *Seramikkusu Ronbunshi*, 1991, **99**(1), 42–46.
7. Mori, T., Yamamura, H., Kobayashi, H. and Mitamura, T., Preparation of high-purity $ZrSiO_4$ powder using sol-gel processing and mechanical properties of the sintered body. *J. Am. Ceram. Soc.*, 1992, **75**, 2420–2426.
8. Itoh, T., Zircon ceramics prepared from hydrous zirconia and amorphous silica. *J. Mater. Sci. Lett.*, 1994, **13**, 1661–1663.
9. Mori T., Yamamura H., Kobayashi H. and Mitamura T. Mechanism formation of $ZrSiO_4$ powders. *J. Mat. Sci.*, 1993, 28, 4970–4973.
10. Shi, Y., Huang, X. and Yan, D., Preparation and characterisation of highly pure fine zircon powder. *J. Europ. Ceram. Soc.*, 1994, **13**(2), 113–119.
11. Tartaj, P., Sanz, J., Serna, J. and Ocana, M., Zircon formation from amorphous spherical $ZrSiO_4$ particles obtained by hydrolysis of aerosols. *J. Mater. Sci.*, 1994, **29**, 6533–6538.
12. Moreno, R., Moya, J. S. and Requena, J., Slip casting of zircon by using an organic surfactant. *Ceram. Internat.*, 1991, **17**, 37–40.
13. Veytizou, C., Quinson, J. F. and Douy, A., Sol-gel synthesis via an aqueous semi-alkoxyde route and characterization of zircon powders. *J. Mater. Chem.*, 2000, **10**, 365–370.
14. Sing, K. S. W., Everett, D. H., Haul, R. A. W., Moscou, L., Pierotti, R. A., Rouquerol, J. and Siemieniewska, T., Reporting physisorption data for Gas/solid systems with special reference to determination of surface area and porosity. *Pure and Appl. Chem.*, 1985, **57**(4), 603–619.
15. Barrett, E. P., Joyner, L. G. and Halenda, P. P., The determination of pore volume and area distributions in porous substances. *I—computations from nitrogen isotherms. J. Am. Chem. Soc.*, 1951, **73**, 373–380.
16. Brunauer, S., Emmett, P. H. and Teller, E., Adsorption of gases in multimolecular layers. *J. Am. Chem. Soc.*, 1938, **60**, 309–319.
17. Lippens, B. C. and De Boer, J. H., Studies on pore systems in catalysts. V—The t method. *J. of catalysis*, 1965, **4**, 319–323.
18. Tang, A., Xu, R., Li, S. and An, Y., Characterization of polymeric reaction in silicic acid solution: intramolecular cyclization. *J. Mater. Chem.*, 1993, **3**, 8 893–896.
19. Benard, P., Louër, M. and Louër, D., Crystal structure determination of $Zr(OH)_2(NO_3)_2$. $4{,}7H_2O$ from X-Ray powder diffraction data. *J. Sol. State Chem.*, 1991, **94**, 27–35.
20. Livage, J., Chatry, M. and Taulelle, F., Complexation of Zr(IV) precursors in aqueous solutions. *Mat. Res. Soc. Symp. Proc*, 1992, **271**, 201–212.
21. Veytizou, C., Valfort, O., Thomas, G. and Quinson, J. F., Zircon formation from amorphous silica and tetragonal zirconia: kinetic study and modelling. *Solid state ionics*, 2001, **139**(3–4), 315–323.
22. Fripiat, J., Chaussidon, J. and Jelli, A., *Chimie-physique des phénomènes de surface. Application aux silicates*. Masson and Cie, Paris, 1971.
23. Glass, S. J. and Ewsuk, K. G., Ceramic powder compaction. *MRS Bulletin*, 1997, **Dec**, 24–28.